ADVANCED MATERIALS
www.advmat.de

How To Quantify the Efficiency Potential of Neat Perovskite Films: Perovskite Semiconductors with an Implied Efficiency Exceeding 28%

Martin Stolterfoht, Max Grischek, Pietro Caprioglio, Christian M. Wolff, Emilio Gutierrez-Partida, Francisco Peña-Camargo, Daniel Rothhardt, Shanshan Zhang, Meysam Raoufi, Jakob Wolansky, Mojtaba Abdi-Jalebi, Samuel D. Stranks, Steve Albrecht, Thomas Kirchartz, and Dieter Neher*

Perovskite photovoltaic (PV) cells have demonstrated power conversion efficiencies (PCE) that are close to those of monocrystalline silicon cells; however, in contrast to silicon PV, perovskites are not limited by Auger recombination under 1-sun illumination. Nevertheless, compared to GaAs and monocrystalline silicon PV, perovskite cells have significantly lower fill factors due to a combination of resistive and non-radiative recombination losses. This necessitates a deeper understanding of the underlying loss mechanisms and in particular the ideality factor of the cell. By measuring the intensity dependence of the external open-circuit voltage and the internal quasi-Fermi level splitting (QFLS), the transport resistance-free efficiency of the complete cell as well as the efficiency potential of any neat perovskite film with or without attached transport layers are quantified. Moreover, intensity-dependent QFLS measurements on different perovskite compositions allows for disentangling of the impact of the interfaces and the perovskite surface on the non-radiative fill factor and open-circuit voltage loss. It is found that potassium-passivated triple cation perovskite films stand out by their exceptionally high implied PCEs > 28%, which could be achieved with ideal transport layers. Finally, strategies are presented to reduce both the ideality factor and transport losses to push the efficiency to the thermodynamic limit.

Within the last years, perovskite semiconductors have been widely applied as active layers in thin film solar cells, as well as in many other opto-electronic devices such as light emitting diodes[1,2] and (photo) detectors.[3–5] Owing to their defect-tolerant nature and ease of fabrication from solution and/or vacuum deposition,[6] perovskites are the almost ideal candidate to be combined with already well-established commercial solar cell technologies such as monocrystalline silicon,[7] CIGS[8] but also with perovskite itself (all-perovskite tandem cells).[9] In the last few years, these properties enabled major research breakthroughs within a comparatively short time which has accelerated research on various PV technologies. For example, with respect to single-junction perovskite solar cells, the efficiency increased from 3.9% to 25.2%[10] within only 10 years and monolithic silicon/perovskite tandem cells reached up to 29.1% power conversion efficiency within an arguably even shorter

Dr. M. Stolterfoht, M. Grischek, P. Caprioglio, C. M. Wolff, E. Gutierrez-Partida, F. Peña-Camargo, D. Rothhardt, S. Zhang, M. Raoufi, J. Wolansky, Prof. D. Neher
Institute of Physics and Astronomy
University of Potsdam
Karl-Liebknecht-Str. 24–25, Potsdam-Golm D-14476, Germany
E-mail: stolterf@uni-potsdam.de

M. Grischek, P. Caprioglio, Prof. S. Albrecht
Young Investigator Group Perovskite Tandem Solar Cells
Helmholtz-Zentrum Berlin für Materialien und Energie GmbH
Kekuléstraße 5, Berlin 12489, Germany

The ORCID identification number(s) for the author(s) of this article can be found under https://doi.org/10.1002/adma.202000080.

DOI: 10.1002/adma.202000080

Dr. M. Abdi-Jalebi, Dr. S. D. Stranks
Cavendish Laboratory
Department of Physics
University of Cambridge
JJ Thomson Avenue, Cambridge CB3 0HE, UK

Dr. M. Abdi-Jalebi
Institute for Materials Discovery
University College London
Torrington Place, London WC1E 7JE, UK

Prof. S. Albrecht
Faculty IV – Electrical Engineering and Computer Science
Technical University Berlin
Berlin 10587, Germany

Prof. T. Kirchartz
Institut für Energie- und Klimaforschung
Forschungszentrum Jülich GmbH
Jülich 52425, Germany

Prof. T. Kirchartz
Faculty of Engineering and CENIDE
University of Duisburg-Essen
Carl-Benz-Str. 199, Duisburg 47057, Germany

time.[10] As with many emerging photovoltaic technologies, a major focus of the research community has been trying to understand the origin of open-circuit voltage losses and a range of different measurement techniques have been proposed to decouple, for example, the contribution of interfacial and bulk recombination on the V_{OC} of the cell.[11–19] These include electrical[19] and all-optical transient measurements such as pump-probe techniques[14–16,20,21]; moreover all-electrical measurements, for example, impedance spectroscopy[15,17,20–22] and optical measurements in steady-state such as photoluminescence spectroscopy.[11–13] Other attempts have been made to explain the dominant recombination mechanism via the ideality factor (n_{ID}) of the complete cell,[11,23–26] however with somewhat limited success considering the difficulty of describing multiple parallel recombination processes in a cell by a single parameter. Today, V_{OC} deficits of only 60 mV with respect to the radiative V_{OC} limit have been reported in literature,[27] which is very close to the theoretical limits and actually already better than monocrystalline Si (green bars in **Figure 1**a). However, the fundamental principles that allowed such low V_{OC} losses are not well understood. In fact, the V_{OC} has been rising so rapidly that in many recent record perovskite cells, the main limiting factor was the fill factor (FF) rather than the V_{OC}.[28,29] This is shown in Figure 1a which demonstrates the significant fraction of FF losses (red bar) with respect to the PCE in the thermodynamic limit in several recent record devices.[30]

In principle, the FF of a working solar cell can be explained by three properties only, that is the charge extraction ability of the cell, the overall Ohmic series resistance and the ideality factor which is defined by the non-radiative recombination processes in the device.[29,31] While the impact of the series resistance can be calculated using Ohm's law, the charge extraction ability depends on the carrier density and the charge carrier mobilities in all stack layers which define the transport resistance ($R_{tr} = d/\sigma$, where d is the film thickness and σ the conductivity).[32,33] In contrast, the non-radiative recombination losses increase the dark current (J_D) and possibly the n_{ID} of the device which will influence the current-density versus voltage curve under illumination and thus the FF. Therefore, there is a direct, well known correlation between the ideality factor and FF.[34] While previous studies have indicated that both the extraction and the ideality factor limit the cell,[29,31] the origin of the ideality factor remains poorly understood which requires a much deeper understanding of the non-radiative recombination pathways. Notably, even in recent record cells with a PCE of 24.2%, a high ideality factor of 1.8 was found which was considered to be one of the main performance limitations of today's perovskite solar cells.[29] Considering, the overall high PCE

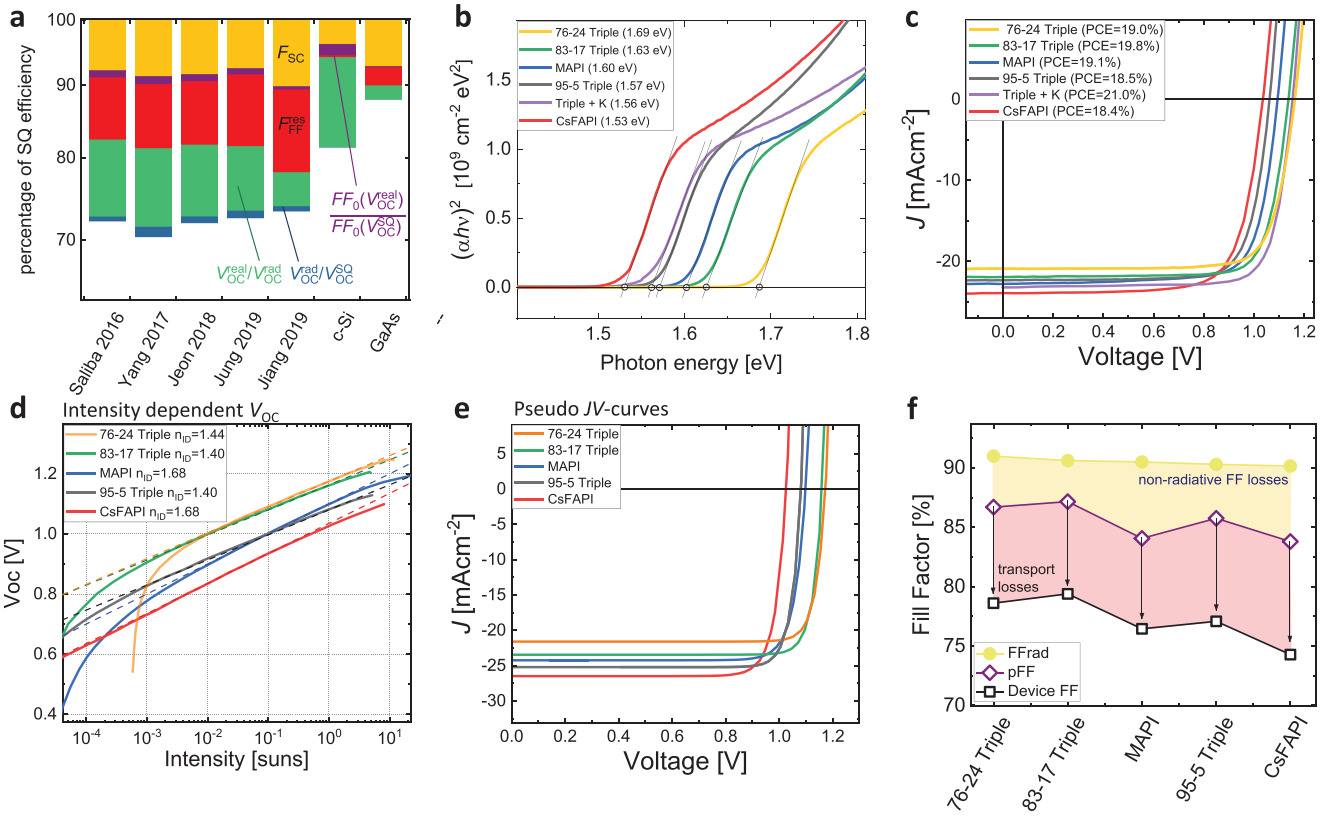

Figure 1. a) Short-circuit current (yellow), open-circuit voltage (V_{OC} green and blue), and fill factor losses (red and purple) in several recent record perovskite solar cells.[28,43,58–61] A similar analysis on a larger set of record devices was recently reported in ref. [28]. In particular, the FF losses are significantly larger then in monocrystalline silicon and GaAs solar cells. b) Tauc plots and c) representative *JV* curves of the studied perovskite films. d) Intensity-dependent V_{OC} and resulting approximation of the ideality factor. e) Pseudo-*JV* (p*JV*) curves of the studied cells as obtained from the intensity-dependent V_{OC}. f) A comparison between the actual device FF and the FF from the p*JV* curves (measured on the same cells), as well as the FF in the radiative limit considering the different bandgaps of the cells.

of state-of-the art perovskite solar cells in numerous research labs today, establishing a detailed understanding of the device operation will become ever more important, as it will become more and more difficult to achieve tangible efficiency increases through trial and error optimizations alone. Arguably, amongst the most pressing questions with regard to understanding the non-radiative recombination processes is the chemical nature of the trap states at the perovskite surfaces.[35,36] For example, why and how exactly most transport layers (TLs) lead to significant additional non-radiative recombination which caps the V_{OC} of many perovskite systems.[15,17,22,37] Moreover, considering the often identical work functions of the contact metals, the origin of any built-in field in perovskite cells is almost entirely unclear, despite its significant impact on the device performance.[37,38] Furthermore, with regard to the ideality factor, the impact of trap states in the bulk and at the interfaces remains poorly understood. In particular, strategies are missing to lower the ideality factor for a given device stack without introducing additional recombination pathways, as well as universal methodologies to limit the recombination at the interfaces and/or in the bulk.[39,40] Clearly, being able to lower the ideality factor to 1 without compromising the V_{OC} and changing the components of the cell would allow one to maximize the PCE of perovskite single-junction cells and to some extent tandem perovskite cells as well.

In this work, we establish a better understanding of how non-radiative recombination in the neat material, the interfaces and/or electrodes defines the fill factor, the ideality factor, and PCE of the complete device. To this end, we quantified in the first part the contribution of charge transport and non-radiative recombination on the FF loss for a series of perovskite solar cells with different bandgaps, following a previous approach based on intensity-dependent V_{OC} measurements. Having identified that non-radiative recombination causes FF losses of ≈ 5% for most compositions, we then aimed to further clarify the contribution of the neat material, the perovskite/TL interfaces and/or the metal contacts on these losses. By measuring the intensity dependence of the QFLS via absolute PL measurements allowed us to experimentally quantify the efficiency potential of any perovskite film on glass in the absence of limiting factors such as transport limitations which could be engineered out in principle. For a triple cation perovskite cell for example, we were able to experimentally determine the PCE losses due to inefficient charge transport, the interfaces and the perovskite surface. For a neat trioctylphosphine oxide (TOPO) passivated triple cation perovskite film, we obtained an implied FF of 88.7% resulting in an implied efficiency of 27.3%. This essentially demonstrates the large efficiency potential of the perovskite bulk with respect to the radiative limit for the given composition with a bandgap of 1.63 eV (30.2%). We then applied this approach to a range of different perovskite compositions with different bandgaps. For a potassium-passivated triple cation perovskite film, we found an even higher efficiency potential exceeding 28% which could be achieved if non-radiative interfacial recombination and charge transport losses could be overcome.

The studied materials of this work include several different perovskite systems with distinct differences in their bandgaps, that is (from high to low bandgap), 1) a "triple cation perovskite" with a nominal composition of $Cs_{0.05}(FA_{0.76}MA_{0.24})_{0.95}Pb(I_{0.76}Br_{0.24})_3$ which comprises $FAPbI_3$ and $MAPbBr_3$ in a ratio of 76:24 and 5 mol% Cs with respect to the other monovalent cations. We note that this composition is suitable for applications in monolithic Si/perovskite tandem solar cells due to its favourable bandgap of ≈ 1.7 eV; 2) a triple cation perovskite as originally proposed by Saliba et al.[41] with a nominal composition of $Cs_{0.05}(FA_{0.83}MA_{0.17})_{0.95}Pb(I_{0.83}Br_{0.17})_3$; 3) a "K-passivated triple cation perovskite" ($Cs_{0.06}FA_{0.79}MA_{0.15}Pb(I_{0.85}Br_{0.15})_3$ + 10 mol% K) with 10 mol% potassium with respect to all other monovalent cations as proposed by Abdi-Jalebi et al.[42] We note that the previous work indicated that potassium is not incorporated into the lattice,[42] and therefore we believe that the above notation is more appropriate; 4) methylammonium lead iodide (MAPI); 5) a "95–5 triple cation perovskite" with a nominal composition of $Cs_{0.05}(FA_{0.95}MA_{0.05})_{0.95}Pb(I_{0.95}Br_{0.05})_3$. Notably, similar compositions are currently employed in many record perovskite devices;[2,43] 6) formamidinium lead iodide (FAPI) with 5 mol% Cs ($Cs_{0.05}FA_{0.95}PI_3$) which was called "CsFAPI." The studied perovskite compositions are listed in **Table 1** and the fabrication details are found in Supporting Information.

For all materials except for the K-passivated triple cation perovskite, *pin*-type perovskite solar cells were fabricated using a thin (8 nm) poly(bis{4-phenyl}{2,4,6-trimethylphenyl}amine) (PTAA) and C_{60} layer (30 nm) as hole and electron transport layer (HTL/ETL), respectively. To improve the wettability of the perovskite layer on PTAA, an ultrathin poly({9,9-bis[3-({*N*,*N*-dimethyl}-*N*-ethylammonium)propyl]-2,7-fluorene}-alt-2,7-{9,9-di-*n*-octylfluorene})dibromide (PFN-Br) layer was added on top of PTAA.[44] Further details are presented in Supporting Information. In contrast, *nip*-type cells were fabricated with K-passivated triple cation perovskite by using TiO_2 and SpiroOMeTAD as electron and hole transport layer, respectively. The bandgaps of the neat materials were obtained from Tauc plots as shown in Figure 1b. Representative *JV* curves of the *pin*-type cells are displayed in the Figure 1c which shows how the differences in the perovskite bandgap translate into different open-circuit voltages and short-circuit currents. A plot of averaged solar cell performance parameters is shown in Figure S1, Supporting Information, and hysteresis *JV*-scans in Figure S2, Supporting Information, which demonstrates the comparatively small hysteresis in this type of *pin*-type cells.

First, in order to estimate the charge-transport losses, intensity-dependent V_{OC} measurements were performed (Figure 1d). The ideality factor was found to be independent of the light exposure time on time scales relevant for the *JV*-scan (0.2 s – 30 s) as

Table 1. Abbreviations of the studied materials and bandgaps obtained from Tauc plots.

Sample ID	Perovskite composition	Bandgap [eV]
76–24 Triple	$Cs_{0.05}(FA_{0.76}MA_{0.24})_{0.95}Pb(I_{0.76}Br_{0.24})_3$	1.69
83–17 Triple	$Cs_{0.05}(FA_{0.83}MA_{0.17})_{0.95}Pb(I_{0.83}Br_{0.17})_3$	1.63
MAPI	$MAPbI_3$	1.60
95–5 Triple	$Cs_{0.05}(FA_{0.95}MA_{0.05})_{0.95}Pb(I_{0.95}Br_{0.05})_3$	1.57
Triple + K	$Cs_{0.06}FA_{0.79}MA_{0.15}Pb(I_{0.85}Br_{0.15})_3$ + 10 mol% K	1.56
CsFAPI	$Cs_{0.05}FA_{0.95}PbI_3$	1.53 eV

exemplified in Figure S3, Supporting Information. Considering that the light intensity is proportional to the generated current density (shown in Figure S4, Supporting Information) allows plotting the V_{OC} as a function of short-circuit current density. If now the *x*-axis is exchanged with the *y*-axis, an exponential current–voltage curve is created that ideally follows the same functional dependence on voltage as the dark current–voltage curve of a diode without any series resistance. Subtracting this from a field-independent charge generation current density (J_G) creates a pseudo-*JV* (p*JV*) curve that is only limited by non-radiative recombination processes in the cell but not by the transport and/or the series resistances (Figure 1e). This is because at V_{OC}, the net current under illumination (= light current) is zero, meaning that transport or series resistances are irrelevant. This can be readily seen from the modified Shockley equation $J_L = -J_G + J_0[\exp((qV - J_L R_{tr/series})/(n_{ID} k_B T)) - 1]$, where J_L, J_G and J_0 are the light, photogenerated and dark saturation current density, respectively; V is the applied voltage; n_{ID} the ideality factor and $R_{tr/series}$ a lumped term describing the transport and/or series resistance.[32,33] This approach has been used in different solar cell technologies to decouple the contribution of FF and charge-transport losses.[11,12,34,45] However, we note that the intensity-dependent V_{OC} is still impacted by energetic offsets between the perovskite and the transport layers which can affect the V_{OC} differently depending on the illumination conditions.[12,37] Nevertheless, the obtained pseudo FF (pFF) for the 83–17 triple cation perovskite cell (87.1%) closely matches the numerically simulated FF in case of infinite mobilities in all layers (87.0%) (Figure S5, Supporting Information).[39,46] Therefore, the difference between the FF from the *JV* curve and the pFF from p*JV* in Figure 1f highlights the FF losses due to inefficient charge transport in all studied cells. Interestingly, a correlation between the non-radiative FF loss and the FF of the complete cell was observed (purple and black points in Figure 1f). This suggests that the FF differences of our devices are primarily due to their different non-radiative recombination losses which comes in addition to a certain FF penalty due to the resistance of the transport layers in the *pin*-type cells. We note that the actual Ohmic series resistance in the small-area devices is very small (≈0.3 Ωcm^2) and not expected to cause significant FF losses as shown in Figure S6, Supporting Information, and further discussed in Note S1, Supporting Information. Moreover, the maximum FF according to the Shockley–Queisser model for all studied cells (with their given bandgap) is approximately 90–91%.[47] Overall, we conclude that the FF is limited due to both insufficient charge extraction and the dark current being higher than the dark current in the radiative limit, that is, due to the presence of additional voltage-dependent non-radiative recombination losses.

While the charge transport losses could be minimized by maximizing the mobilities in the hole transport layer and the perovskite layer by roughly a factor of 10 (Figure S5, Supporting Information), this has been proven difficult to realize experimentally. Therefore, in the following we aim to understand the factors limiting the ideality factor of our cells which may provide new, unexpected optimization strategies. To this end, we fabricated for each system the neat materials on a glass substrate, the optical *pin*-stack (i.e., the perovskite sandwiched between the electron and hole transport layers), as well as the complete cells between an ITO and Cu contact. For some compositions, we further investigated the perovskite with either the HTL or the ETL on top. In analogy of using $V_{OC}(I)$ to access the pFF of a complete cell in the absence of transport limitations, we can use the intensity dependence of the QFLS to quantify the pFF or the efficiency potential of any perovskite film with or without transport layers.[12] As discussed in earlier works, we obtain the QFLS from the equation $QFLS = k_B T \ln(PLQY \times J_G/J_{0,rad})$, where the PLQY is the PL quantum yield efficiency, J_G the generated current density at 1 sun and $J_{0,rad}$ the radiative recombination current in the dark.[48,49] Details about this approach are presented in Note S2, Supporting Information, while the parameters used J_G and $J_{0,rad}$ are provided in Table S1 and Figure S7, Supporting Information. **Figure 2**a shows the emitted PL for a neat perovskite film under a 1 sun equivalent illumination through a long-pass filter of 600 nm. Measuring the absolute emitted photon flux as a function of illumination intensity allows quantifying of the intensity-dependent QFLS. This is illustrated schematically in Figure 2b which shows a generic band diagram of a neat perovskite film and the simulated QFLS as a function of the light intensity from 0.001 to 10 suns where recombination happens within the bulk and at the right surface with a recombination velocity of 1000 cm s^{-1}.[37,50] We note that this is merely an illustration and is not at this point intended to reproduce the situation in an actual measurement. Considering again that the intensity is directly proportional to the generated current density in the film and that the QFLS is the internal voltage (times the elementary charge *e*), we can plot a QFLS – J_{SC} diagram and subsequently create a pseudo-*JV* curve of a neat triple cation perovskite film (Figure 2d–f). This analysis yields an implied efficiency of roughly ≈ 25% for a neat triple cation perovskite film, which could be achieved if non-radiative recombination happens only in the bulk but not across the interfaces and in the absence of transport losses or series resistance limitations. Although certainly optimistic, we believe that this is possible considering that in other inorganic solar cells, the charge transport layers actually passivate (improve) the non-radiative recombination at the surfaces and thus the quality of the absorber layer.

In the next part, we aim to further understand the implied efficiency potential of all neat perovskite layers considered in this study. The intensity-dependent QFLS of all neat materials is shown in **Figure 3**a, which highlights significant differences in the QFLS under 1 sun equivalent conditions, however, there are also distinct differences in the ideality factors. For example, the K-passivated triple cation perovskite exhibits an average ideality factor of approximately 1.35 from 0.01 to 1 sun, while neat CsFAPI with the lowest PLQY exhibits a value close to 2. The n_{ID} is ≈ 1.4–1.5 for the other samples. Possible factors influencing the n_{ID} in the neat material are discussed further below. Figure 3b and **Table 2** show the corresponding p*JV* curves of the neat materials, which highlights the significantly higher efficiency potential in the K-passivated triple cation perovskite. This composition has been previously introduced and PLQY values of up to 66% have been reported which was attributed to an effective passivation of grain boundaries through the potassium.[42] In order to then determine the efficiency potential of the sample, we need to make an optimistic but still realistic assumption for the external photovoltaic quantum efficiency

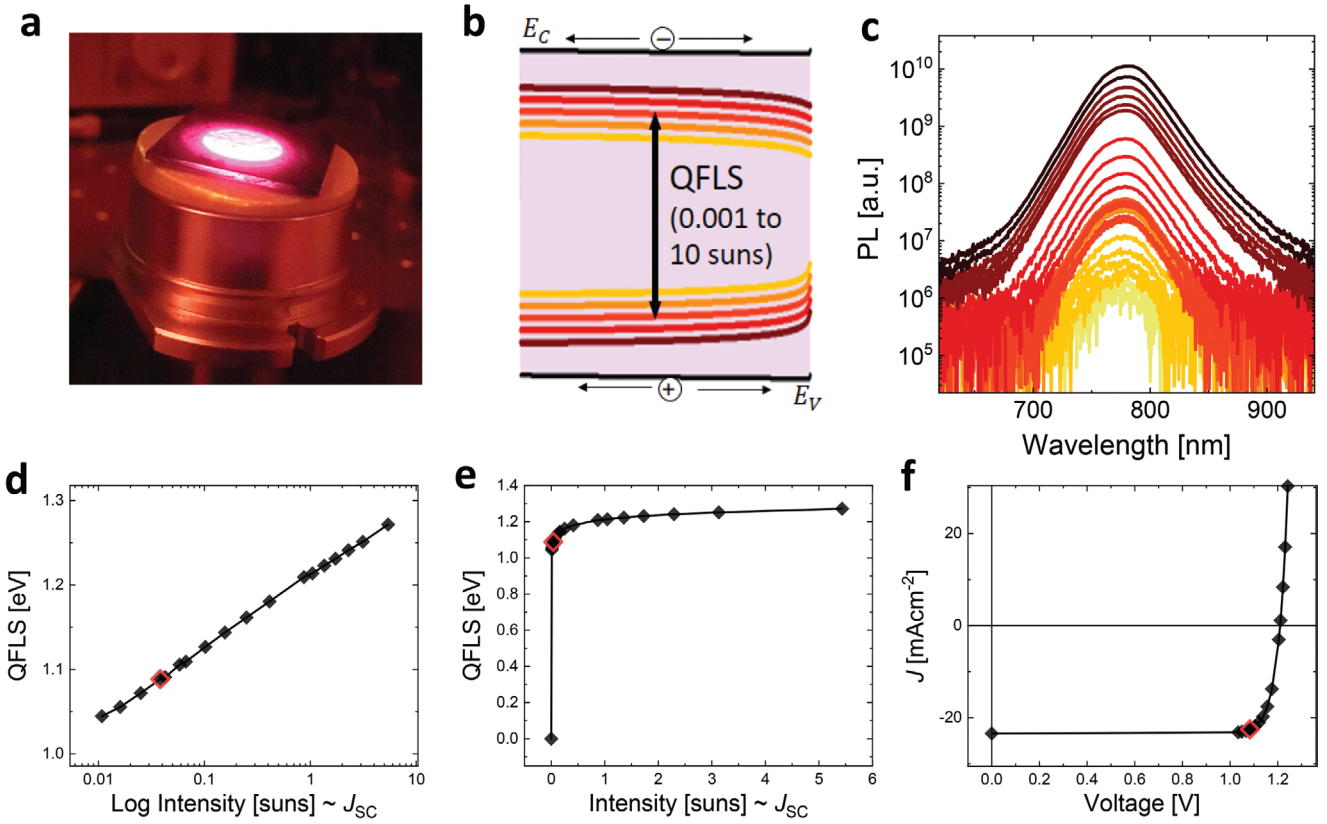

Figure 2. a) Image of the photoluminescence of a perovskite film under a 1 sun illumination through a 600 nm cut-off filter. b) A simulation of the intensity-dependent QFLS in a neat film at different illumination intensities. c) Intensity-dependent PL spectra as obtained on a neat triple cation perovskite film from < 0.01 to 1 sun. d) The obtained QFLS as a function of light intensity which is directly proportional to the generated current under short-circuit conditions. e) The internal voltage (=QFLS/*e*) versus the short-circuit current density in a lin-lin representation. f) The obtained pseudo *JV* curve of a neat triple cation perovskite film. Measurement of the QFLS as a function of light intensity allows to quantify the implied efficiency of a neat material that is only limited by the non-radiative recombination processes taking place in the bulk and its surface in absence of across-interface recombination and/or charge transport losses. The maximum power point is marked in red in panel (d–f).

(EQE) of the cell above the gap. Using a value of EQE = 95% that has already been reached experimentally[51] but still represents a very optimistic and ambitious target, the K-passivated triple cation perovskite exhibits an efficiency potential of 28.2%. When considering that non-radiative interfacial recombination losses are rather small in this system as shown previously, this would suggest that this efficiency could be achieved if energy level alignment issues between the perovskite and the charge transport layers were overcome and transport limitations were minimized. At this point, we note that time-dependent

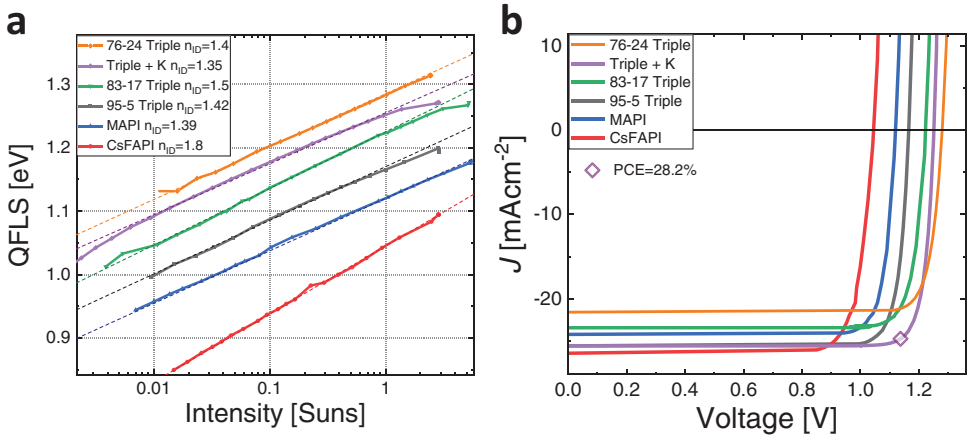

Figure 3. a) Intensity-dependent quasi-Fermi level splitting and resulting ideality factors of the neat perovskite films discussed in this study. b) The corresponding pseudo-*JV* curves of the neat materials highlight the exceptional efficiency potential of K-passivated triple cation perovskite absorbers.

Table 2. Performance parameters deduced from the p*JV* curves of the neat perovskite layers and the measured ideality factor and PLQY.

Sample	pJ_{SC} [mA cm^{-2}]	pV_{OC} [V]	pFF [%]	pPCE [%]	$\approx n_{ID}$	PLQY [%]
76–24 Triple	21.60	1.283	87.3	24.2	1.40	0.9
83–17 Triple	23.45	1.220	86.5	24.8	1.50	1.0
MAPI	24.24	1.124	86.4	23.5	1.39	0.039
95–5 Triple	25.61	1.163	86.7	25.8	1.42	0.98
Triple + K	25.61	1.252	88.0	28.2	1.35	27.7
CsFAPI	26.48	1.044	82.5	22.8	1.80	0.018

phenomena are always an important consideration in perovskite solar cells.[52–56] Therefore, in order to correlate the optical and the electrical measurements, we performed the intensity-dependent QFLS measurements for different exposure times, ranging from 0.4 s to 30 s at each measured data point which is relevant for the typical timescales of *JV*-scans. Figures S8 and S9, Supporting Information, show that the obtained ideality factor and pFF is essentially independent of exposure time within the studied time range which confirms the robustness of our approach.

While Figure 3 highlighted the substantial efficiency potential of the neat perovskite absorber layers, in the next step, we aim to untangle the limiting factors determining the FF and V_{OC} losses of the triple cation perovskite cells. To this end, we quantified the efficiency potential of the individual perovskite/transport layer combinations of the cell using again intensity-dependent QFLS measurements. **Figure 4**a shows the *JV* curve of the standard cell compared to the p*JV* curve from the intensity-dependent V_{OC}. In addition, the graph shows the p*JV* curves of the perovskite/C_{60} junction, the optical *pin*-stack (glass/PTAA/PFN-Br/perovskite/C_{60}), the neat film, the neat passivated perovskite film with TOPO[36,57] as obtained from the QFLS(*I*) (assuming an EQE of 95%), and finally the curve in the radiative (Shockley–Queisser) limit for the bandgap of the studied composition. Figure 4b highlights the (implied) FFs and open-circuit voltages and Figure 4c and d show a zoom of the region around the maximum power point to better highlight the individual impact of the efficiency limiting processes on the V_{OC} and the FF. All implied performance parameters from the intensity-dependent measurements on the different stack layers of the 83–17 triple cation system are summarized in **Table 3**. While the difference between the *JV* curve (PCE = 21.2% assuming an EQE of 95%) and the p*JV* curve from the $V_{OC}(I)$ measurement (pPCE = 23.7%) shows the transport losses in the cell (blue color in panel c), we find that the p*JV* curve from the V_{OC} measurement is also nearly identical to the p*JV* curve of the *pin*-stack (pPCE = 23.5%) as obtained from the QFLS(*I*). This indicates that in this device, electrode-induced non-radiative losses are negligible; this observation is also interesting with respect to the origin of the built-in field in perovskite cells, which we will discuss further below. Moreover, the p*JV* curve of the optical *pin*-stack is essentially identical to the p*JV* curve of the perovskite/C_{60} film (pPCE = 23.5%). This highlights that the C_{60} interface dominates the recombination loss in the complete cell, consistent with our previous results.[37] The additional loss of ≈ 67 mV due to the C_{60} interface can be estimated from the difference between the p*JV* curve of the neat material (pPCE = 24.8%) and the pero/C_{60} film (purple color in panel c). Finally, regarding the neat passivated perovskite film with an implied PCE of 27.3%, if one assumes that TOPO passivates only defects at the top surface as concluded previously,[57] we could tentatively assign the difference between the neat and the passivated neat film to surface recombination (red color in panel (c)). Interestingly, Figure 4b shows that the pFF is roughly the same in the neat material, the perovskite/C_{60} film and in the *pin*-stack, however upon the passivation also the pFF increases by roughly 2% (to 88.7%) which brings the efficiency potential very close to the radiative limit (orange color in panel c) for the given bandgap. In this regard, it is also interesting to note that the PLQY of the TOPO-passivated 83–17 triple cation film is as high as 22.6% as compared to 0.8% of the unpassivated film. Notably, this PLQY enhancement is similar to previous results where TOPO was applied on top of MAPI,[36,57] indicating that TOPO passivates similar surface defects in case of (83–17) triple

Table 3. Implied performance parameters deduced from the *JV* and p*JV* curves of different stack layers of the triple cation system as well as the measured PLQY and the assigned primary limitation.

Sample	Method	pV_{OC} [V]	pFF [%]	pPCE [%]	PLQY [%]	Primary limitation
Cell	*JV*	1.138	79.4	21.2[a)]		Transport, interface[a)]
Cell	$V_{OC}(I)$	1.159	87.1	23.7		Interface
Pero/C_{60}	QFLS(*I*)	1.153	86.9	23.5	0.058	Interface
pin-stack	QFLS(*I*)	1.157	86.7	23.5	0.068	Interface
Pero	QFLS(*I*)	1.220	86.5	24.8	0.78	Surface
Pero/TOPO	QFLS(*I*)	1.310	88.7	27.3	22.6	Bulk and/or surface

[a)]The J_{SC} of all samples was set to 23.45 mA cm^{-2} (EQE = 95%) to limit the discussion here to FF and V_{OC} losses. The actual J_{SC} of the 83–17 triple cation cell is 21.9 mA cm^{-2} (PCE = 19.8%); therefore, the cell is also limited by optical losses and EQE losses more generally.

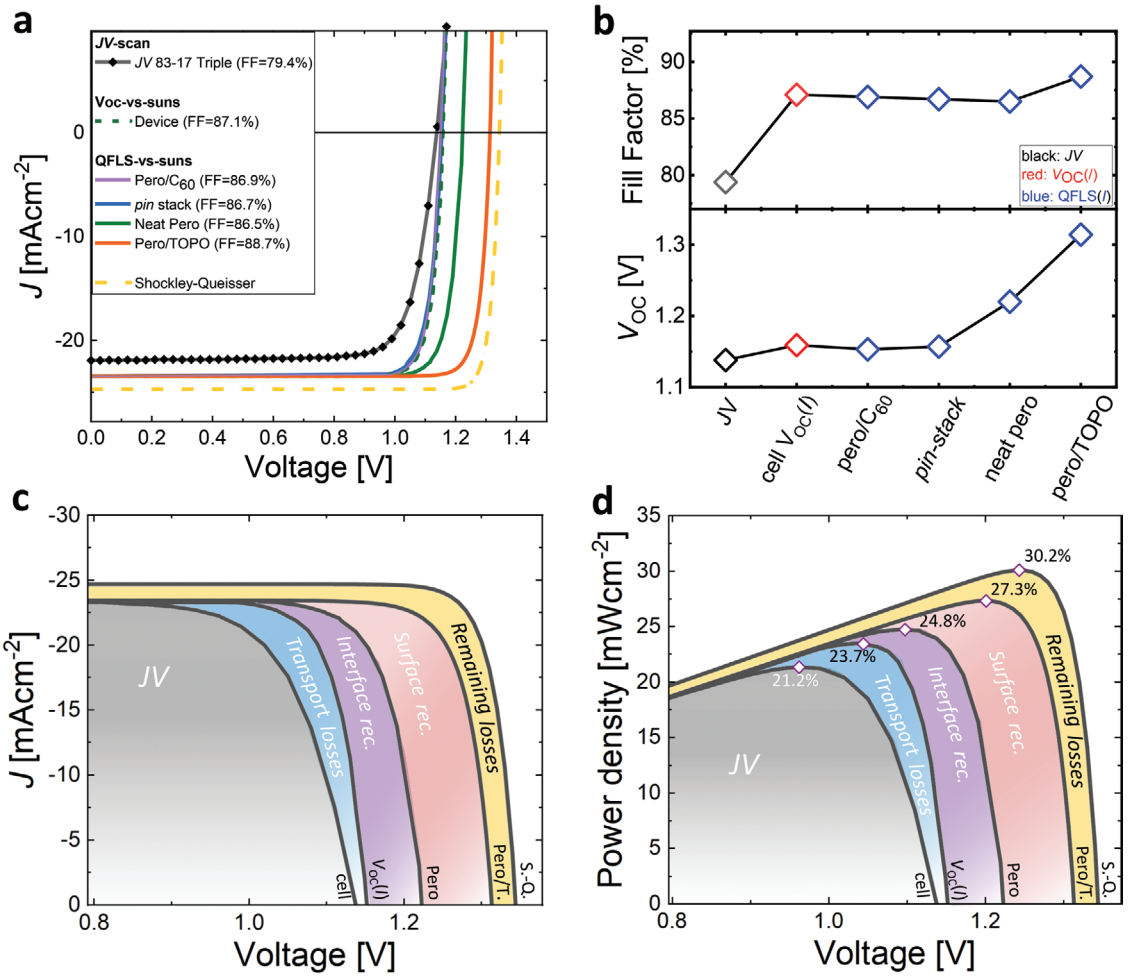

Figure 4. a) Current-density versus voltage (*JV*) characteristics of triple cation cells (black line) compared to pseudo-*JV* (p*JV*) curves obtained from intensity-dependent $V_{OC}(I)$ (dashed line) and QFLS measurements on the neat perovskite, the perovskite/C_{60}, the optical *pin*-stack and the complete cell (solid lines). b) The implied FF and open-circuit voltage of the individual films. c,d) *JV* curves untangling the loss mechanisms due to insufficient charge transport (difference between the *JV* and the p*JV* curve from the intensity-dependent V_{OC}); interfacial losses (difference of the p*JV* curve of the neat material and the optical *pin*-stack on glass); losses at the perovskite surface (difference between the p*JV* curve of the neat and the passivated neat material); and the remaining losses in the passivated perovskite (i.e., bulk and/or surface recombination). We note an EQE of 95% was assumed for all *JV* and p*JV* curves except for the Shockley–Queisser curve to limit the discussion here to FF and V_{OC} losses. Note, the p*JV* curve of the optical *pin*-stack is nearly identical to the p*JV* curve from $V_{OC}(I)$ and therefore not shown in (c) and (d) for simplicity. Panel (d) also highlights the implied efficiency at the maximum power point for each sample allowing to read off the induced efficiency losses due to the different recombination processes.

cation perovskite and MAPI. Moreover, this suggests that the recombination in the perovskite bulk is very small compared to the recombination at the surface (in fact, ≈30 times smaller when comparing the PLQY of the neat and the passivated neat sample in Table 3). Nevertheless, we acknowledge that so far and to our knowledge, TOPO has not been proven to be an effective passivation strategy in complete cells as it possibly forms an insulation barrier that also blocks majority carriers from being efficiently extracted. One should therefore seek similar passivation strategies that provide similarly high luminescence yields without impeding charge transport and collection behavior.

In the following, we further analyze the results on different layer stacks for other perovskite compositions that are part of the study in order to identify common trends for different systems. **Figure 5** shows the pFF as obtained from the intensity-dependent V_{OC} and QFLS measurements in the neat material, the *pin*-stack, and the complete cell. The corresponding p*JV* and n_{ID} values are shown in Figures S10 and S11, Supporting Information, respectively. As expected, the pFF of the neat material is significantly higher than the device FF. Interestingly, however, addition of the TLs to the neat material ("*pin*-stack") leads to different effects. In case of MAPI (green line) it slightly lowers the pFF and increases the n_{ID}, while the opposite is the case for CsFAPI (red line), where the transport layers increase the pFF and lower the n_{ID}. Overall, Figure 5 shows that the pFF is rather similar for different stack layers which indicates that it is mostly the neat material (or the perovskite surface) which defines the non-radiative FF loss in the complete cell (Figure 1f). Especially, in case of the triple cation perovskites (76:24, 83:17, and 95:5), the addition of both transport layers

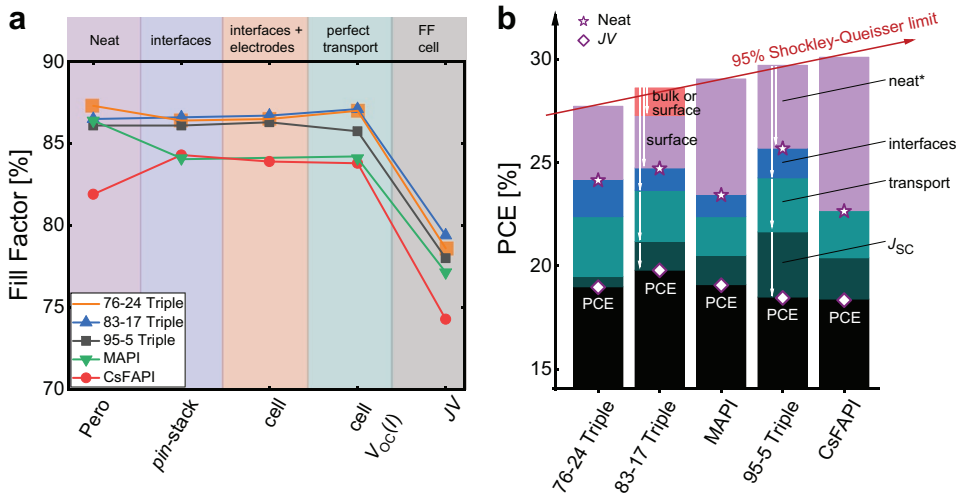

Figure 5. a) The pseudo fill factor (pFF) of the neat perovskite material, the *pin*-stack on glass (without electrodes), and the complete cell (transport layers + electrodes) as obtained from the intensity-dependent QFLS for different perovskite compositions. Also shown are the pFF of the complete cell from the intensity-dependent V_{OC} which represents the non-radiative recombination limited FF in absence of transport limitations and the device fill factor. b) A summary of the main efficiency losses in the perovskite systems discussed in this study due to short-circuit current losses (difference between the measured J_{SC} and the J_{SC} with an average EQE of 95%), insufficient charge transport (as discussed for instance in Figure 1f), interface recombination (difference between the implied efficiency of the neat material and the *pin*-stack), and implied PCE losses in the neat material with respect to 95% of the Shockley–Queisser limit. *Note that except for the 83–17 triple cation perovskite system, we have not attempted to further decouple the pseudo efficiency losses in the neat material into contributions of bulk and surface recombination. Moreover, it is important to note that losses in the neat material (bulk or surface) and the interfaces are not cumulative, meaning that these parts limit the performance to certain value.

has little impact. On the other hand, the FF from the *JV*-curve always lies below the pFF of the complete cell, highlighting the significance of transport losses in all devices. Figure 5b shows a comparison of the major PCE efficiency losses in the studied perovskite systems in analogy to the approach presented in Figure 4 (see Figure S10, Supporting Information, for the p*JV* of the other systems). Note that the PCE comprises both fill factor and V_{OC} losses and that for most systems the V_{OC} loss is dominated by interface recombination rather than bulk properties. Therefore, PCE losses in the neat material and the interface are not additive, meaning that improvements in the bulk alone will, in principal, not allow performance improvements. This is also due to the logarithmic dependence of the V_{OC} (and therefore the PCE) on the recombination currents in the perovskite bulk, surface and interfaces. Therefore, these components of the cell limit the obtainable PCE to a certain value.

Lastly, coming back to the observation that the presence of the metal electrodes has a small impact on the ideality factor (Figure S11, Supporting Information) and the pFF, this may suggest that the built-in potential (V_{BI}) of the cell is not significantly altered upon the addition of the electrodes. This is because n_{ID} depends strongly on the V_{BI} (Figure S12, Supporting Information) as it physically separates electrons and holes depending on the illumination intensity and on the resulting QFLS and band bending. For example, in the case of an intrinsic semiconductor with mid-gap traps and Shockley–Read–Hall recombination, the ideality factor would be exactly 2 in the absence of a built-in field. However, it can approach a value of 1 when the eV_{BI} approaches the bandgap of the perovskite. Therefore, these results are not consistent with the assumption that an effective difference in the metal workfunctions defines the built-in field of the perovskite solar cell as this would lead to changes in n_{ID} when going from the optical stack on glass to the complete cell. While this observation will require further investigations, our results suggest the importance of a high built-in field across the perovskite absorber not only to minimize the transport losses (as a strong V_{BI} is beneficial to drive the carriers to the selective contacts, minimizing the decisive interfacial recombination) but also to lower the ideality factor, thereby reducing the dark recombination current.[39]

In this work, we have studied the impact of non-radiative recombination on the FF losses for a series of perovskite compositions with different band gaps. Intensity-dependent V_{OC} measurements allowed us to disentangle the contribution of non-radiative recombination and transport losses on the device FF. Consistent with previous studies, we identified that the FF is limited by both of these loss mechanisms, underlining the need for a deeper understanding of the ideality factor in perovskite solar cells. Intensity-dependent QFLS measurements on individual perovskite/transport layer films comprising the cell allow for a closer look into parameters determining the ideality factor and provide experimental means to directly quantify the PCE potential of any perovskite/transport layer film on glass. We demonstrated the suitability of the proposed approach for efficient triple cation perovskite cells (PCE = 19.8%). Using this method, we found that the implied efficiency of the perovskite/C_{60} junction (23.5%) is nearly identical to the optical *pin*-stack on glass (23.5%) and the complete cell (23.7%) as obtained from the V_{OC} versus suns method, but lower than the implied efficiency of the neat material (24.8%). As such, these measurements revealed the efficiency limitations imposed by interfacial recombination (in particular at the C_{60} interface), while the application of TOPO on top of the perovskite increased the PLQY to 22.6% and the implied FF and efficiency to 88.7% and 27.3%, respectively. These results thereby demonstrated the limitation due

to surface recombination and the efficiency potential when surface and interfacial recombination are minimized. To generalize the results, we further studied several other perovskite compositions where we found that the addition of the transport layers to the absorber layer has some effect on the pFF and the n_{ID} in case of MAPI and CsFAPI cells. However, in the triple cation perovskite systems, the pFF of the cell is similar to that of the unpassivated neat material where we expect that most recombination happens at the perovskite surface. We also discussed the importance of the built-in field across the perovskite layer to reduce both the charge-transport losses and the ideality factor of the complete cells. Finally, we experimentally demonstrated the high efficiency potential of all studied neat perovskite films that could be reached upon minimization of interfacial recombination and by enhancing the carrier mobilities by roughly a factor of 10, and/or through TL doping. In particular, the efficiency potential of K-passivated triple cation perovskite films was quantified to be above 28%, which promises further efficiency gains in the near future through better energy alignment and optimization of the mobilities and/or conductivities in the stack layers.

Supporting Information

Supporting Information is available from the Wiley Online Library or from the author.

Acknowledgements

This work was in part funded by HyPerCells (a joint graduate school of the Potsdam University and the Helmholtz-Zentrum Berlin) and by the Deutsche Forschungsgemeinschaft (DFG, German Research Foundation): project number 423749265. S.D.S. acknowledges funding from the Royal Society and Tata Group (UF150033) and the Engineering and Physical Sciences Research Council (EP/R023980/1). M.A.-J. acknowledges EPSRC, Cambridge Materials Limited and Wolfson College, University of Cambridge for their funding and technical support. M.G., P.C., S.A., and D.N. acknowledge funding from the Helmholtz Association via HI-SCORE (Helmholtz International Research School). M.G., P.C., and S.A. acknowledge the Federal Ministry of Education and Research (BMBF) for funding of the Young Investigator Group Perovskite Tandem Solar Cells within the program "Materialforschung fuer die Energiewende" (grant no. 03SF0540). The authors thank Nandi Wu, Daniel Walter, and Klaus Weber from the Australian National University for help and fruitful discussions.

Conflict of Interest

The authors declare no conflict of interest.

Keywords

non-radiative interface recombination, perovskite solar cells, photoluminescence

Received: January 4, 2020
Revised: February 13, 2020
Published online:

[1] Y. Cao, N. Wang, H. Tian, J. Guo, Y. Wei, H. Chen, Y. Miao, W. Zou, K. Pan, Y. He, H. Cao, Y. Ke, M. Xu, Y. Wang, M. Yang, K. Du, Z. Fu, D. Kong, D. Dai, Y. Jin, G. Li, H. Li, Q. Peng, J. Wang, W. Huang, *Nature* **2018**, *562*, 249.
[2] W. Xu, Q. Hu, S. Bai, C. Bao, Y. Miao, Z. Yuan, T. Borzda, A. J. Barker, E. Tyukalova, Z. Hu, M. Kawecki, H. Wang, Z. Yan, X. Liu, X. Shi, K. Uvdal, M. Fahlman, W. Zhang, M. Duchamp, J.-M. Liu, A. Petrozza, J. Wang, L.-M. Liu, W. Huang, F. Gao, *Nat. Photonics* **2019**, *13*, 418.
[3] Q. Lin, A. Armin, P. L. Burn, P. Meredith, *Nat Phot.* **2015**, *9*, 687.
[4] D. M. Lyons, A. Armin, M. Stolterfoht, R. C. R. Nagiri, R. D. J. van Vuuren, B. N. Pal, P. L. Burn, S.-C. Lo, P. Meredith, *Org. Electron.* **2014**, *15*, 2903.
[5] L. Dou, Y. M. Yang, J. You, Z. Hong, W. H. Chang, G. Li, Y. Yang, *Nat. Commun.* **2014**, *5*, 5404.
[6] M. Liu, M. B. Johnston, H. J. Snaith, *Nature* **2013**, *501*, 395.
[7] F. Sahli, J. Werner, B. A. Kamino, M. Bräuninger, R. Monnard, B. Paviet-Salomon, L. Barraud, L. Ding, J. J. Diaz Leon, D. Sacchetto, G. Cattaneo, M. Despeisse, M. Boccard, S. Nicolay, Q. Jeangros, B. Niesen, C. Ballif, *Nat. Mater.* **2018**, *17*, 820.
[8] A. Al-Ashouri, A. Magomedov, M. Roß, M. Jošt, M. Talaikis, G. Chistiakova, T. Bertram, J. A. Márquez, E. Köhnen, E. Kasparavičius, S. Levcenco, L. Gil-Escrig, C. J. Hages, R. Schlatmann, B. Rech, T. Malinauskas, T. Unold, C. A. Kaufmann, L. Korte, G. Niaura, V. Getautis, S. Albrecht, *Energy Environ. Sci.* **2019**, *12*, 3356.
[9] R. Lin, K. Xiao, Z. Qin, Q. Han, C. Zhang, M. Wei, M. I. Saidaminov, Y. Gao, J. Xu, M. Xiao, A. Li, J. Zhu, E. H. Sargent, H. Tan, *Nat. Energy* **2019**, *4*, 864.
[10] NREL, *Best Research-Cell Efficiencies*, https://www.nrel.gov/pv/cell-efficiency.html (accessed: September 2019).
[11] V. Sarritzu, N. Sestu, D. Marongiu, X. Chang, S. Masi, A. Rizzo, S. Colella, F. Quochi, M. Saba, A. Mura, G. Bongiovanni, *Sci. Rep.* **2017**, *7*, 44629.
[12] N. Wu, Y. Wu, D. Walter, H. Shen, T. Duong, D. Grant, C. Barugkin, X. Fu, J. Peng, T. White, K. Catchpole, K. Weber, *Energy Technol.* **2017**, *5*, 1827.
[13] M. Stolterfoht, C. M. Wolff, J. A. Márquez, S. Zhang, C. J. Hages, D. Rothhardt, S. Albrecht, P. L. Burn, P. Meredith, T. Unold, D. Neher, *Nat. Energy* **2018**, *3*, 847.
[14] F. Staub, H. Hempel, J. C. Hebig, J. Mock, U. W. Paetzold, U. Rau, T. Unold, T. Kirchartz, *Phys. Rev. Appl.* **2016**, *6*, 044017.
[15] C. M. Wolff, F. Zu, A. Paulke, L. P. Toro, N. Koch, D. Neher, *Adv. Mater.* **2017**, *29*, 1700159.
[16] B. Krogmeier, F. Staub, D. Grabowski, U. Rau, T. Kirchartz, *Sustain. Energy Fuels* **2018**, *2*, 1027.
[17] J.-P. Correa-Baena, W. Tress, K. Domanski, E. H. Anaraki, S.-H. Turren-Cruz, B. Roose, P. P. Boix, M. Grätzel, M. Saliba, A. Abate, A. Hagfeldt, *Energy Environ. Sci.* **2017**, *10*, 1207.
[18] E. Guillén, F. J. Ramos, J. A. Anta, S. Ahmad, E. Guille, F. J. Ramos, J. A. Anta, S. Ahmad, *J. Phys. Chem. C* **2014**, *118*, 22913.
[19] D. Kiermasch, A. Baumann, M. Fischer, V. Dyakonov, K. Tvingstedt, *Energy Environ. Sci.* **2018**, *11*, 629.
[20] E. M. Hutter, J. J. Hofman, M. L. Petrus, M. Moes, R. D. Abellón, P. Docampo, T. J. Savenije, *Adv. Energy Mater.* **2017**, *7*, 1602349.
[21] Y. Yang, M. Yang, D. T. Moore, Y. Yan, E. M. Miller, K. Zhu, M. C. Beard, *Nat. Energy* **2017**, *2*, 1.
[22] K. Tvingstedt, L. Gil-Escrig, C. Momblona, P. Rieder, D. Kiermasch, M. Sessolo, A. Baumann, H. J. Bolink, V. Dyakonov, *ACS Energy Lett.* **2017**, *2*, 424.
[23] G. J. A. H. Wetzelaer, M. Scheepers, A. M. Sempere, C. Momblona, J. Ávila, H. J. Bolink, *Adv. Mater.* **2015**, *27*, 1837.
[24] W. Tress, M. Yavari, K. Domanski, P. Yadav, B. Niesen, J.-P. Correa-Baena, A. Hagfeldt, M. Graetzel, *Energy Environ. Sci.* **2018**, *11*, 151.

[25] T. Kirchartz, F. Deledalle, P. S. Tuladhar, J. R. Durrant, J. Nelson, *J. Phys. Chem. Lett.* **2013**, *4*, 2371.
[26] P. Calado, D. Burkitt, J. Yao, J. Troughton, T. M. Watson, M. J. Carnie, A. M. Telford, B. C. O. Regan, J. Nelson, P. R. F. Barnes, *Phys. Rev. Appl.* **2019**, *10*, 044005.
[27] Z. Liu, L. Krückemeier, B. Krogmeier, B. Klingebiel, J. A. Márquez, S. Levcenko, S. Öz, S. Mathur, U. Rau, T. Unold, T. Kirchartz, *ACS Energy Lett.* **2019**, *4*, 110.
[28] L. Krückemeier, U. Rau, M. Stolterfoht, T. Kirchartz, *Adv. Energy Mater.* **2020**, *10*, 1902573.
[29] M. A. Green, A. W. Y. Ho-Baillie, *ACS Energy Lett.* **2019**, 1639.
[30] J. F. Guillemoles, T. Kirchartz, D. Cahen, U. Rau, *Nat. Photonics* **2019**, *13*, 501.
[31] M. Stolterfoht, C. M. Wolff, Y. Amir, A. Paulke, L. Perdigón-Toro, P. Caprioglio, D. Neher, *Energy Environ. Sci.* **2017**, *10*, 1530.
[32] U. Würfel, D. Neher, A. Spies, S. Albrecht, *Nat. Commun.* **2015**, *6*, 6951.
[33] D. Neher, J. Kniepert, A. Elimelech, L. J. A. Koster, *Sci. Rep.* **2016**, *6*, 24861.
[34] M. A. Green, *Sol. Cells* **1983**, *7*, 337.
[35] B. Chen, P. N. Rudd, S. Yang, Y. Yuan, J. Huang, *Chem. Soc. Rev.* **2019**, *48*, 3842.
[36] I. L. Braly, H. W. Hillhouse, *J. Phys. Chem. C* **2016**, *120*, 893.
[37] M. Stolterfoht, P. Caprioglio, C. M. Wolff, J. A. Márquez, J. Nordmann, S. Zhang, D. Rothhardt, U. Hörmann, Y. Amir, A. Redinger, L. Kegelmann, F. Zu, S. Albrecht, N. Koch, T. Kirchartz, M. Saliba, T. Unold, D. Neher, *Energy Environ. Sci.* **2019**, *12*, 2778.
[38] T. Kirchartz, *Philos. Trans. R. Soc. A Math. Phys. Eng. Sci.* **2019**, *377*, 20180286.
[39] J. Diekmann, P. Caprioglio, D. Rothhardt, M. Arvind, T. Unold, T. Kirchartz, D. Neher, M. Stolterfoht, ArXiv: 1910.07422 [cond-mat.mtrl-sci], **2019**.
[40] W. Tress, *Adv. Energy Mater.* **2017**, *7*, 1602358.
[41] M. Saliba, T. Matsui, J.-Y. Seo, K. Domanski, J.-P. Correa-Baena, M. K. Nazeeruddin, S. M. Zakeeruddin, W. Tress, A. Abate, A. Hagfeldt, M. Grätzel, *Energy Environ. Sci.* **2016**, *9*, 1989.
[42] M. Abdi-Jalebi, Z. Andaji-Garmaroudi, S. Cacovich, C. Stavrakas, B. Philippe, J. M. Richter, M. Alsari, E. P. Booker, E. M. Hutter, A. J. Pearson, S. Lilliu, T. J. Savenije, H. Rensmo, G. Divitini, C. Ducati, R. H. Friend, S. D. Stranks, *Nature* **2018**, *555*, 497.
[43] N. J. Jeon, H. Na, E. H. Jung, T.-Y. Yang, Y. G. Lee, G. Kim, H.-W. Shin, S. Il Seok, J. Lee, J. Seo, *Nat. Energy* **2018**, *3*, 682.
[44] J. Lee, H. Kang, G. Kim, H. Back, J. Kim, S. Hong, B. Park, E. Lee, K. Lee, *Adv. Mater.* **2017**, *29*, 1606363.
[45] J. Greulich, M. Glatthaar, S. Rein, *Prog. Photovoltaics Res. Appl.* **2010**, *18*, 511.
[46] M. Burgelman, P. Nollet, S. Degrave, *Thin Solid Films* **2000**, *362*, 527.
[47] S. Rühle, *Sol. Energy* **2016**, *130*, 139.
[48] W. Tress, N. Marinova, O. Inganäs, M. K. Nazeeruddin, S. M. Zakeeruddin, M. Graetzel, *Adv. Energy Mater.* **2015**, *5*, 1400812.
[49] K. Tvingstedt, O. Malinkiewicz, A. Baumann, C. Deibel, H. J. Snaith, V. Dyakonov, H. J. Bolink, *Sci. Rep.* **2014**, *4*, 6071.
[50] J. Wang, W. Fu, S. Jariwala, I. Sinha, A. K. Y. Jen, D. S. Ginger, *ACS Energy Lett.* **2019**, *4*, 222.
[51] M. Kim, G.-H. Kim, T. K. Lee, I. W. Choi, H. W. Choi, Y. Jo, Y. J. Yoon, J. W. Kim, J. Lee, D. Huh, H. Lee, S. K. Kwak, J. Y. Kim, D. S. Kim, *Joule* **2019**, *3*, 2179.
[52] S. A. L. Weber, I. M. Hermes, S. H. Turren-Cruz, C. Gort, V. W. Bergmann, L. Gilson, A. Hagfeldt, M. Graetzel, W. Tress, R. Berger, *Energy Environ. Sci.* **2018**, *11*, 2404.
[53] G. Richardson, S. E. J. O'Kane, R. G. Niemann, T. A. Peltola, J. M. Foster, P. J. Cameron, A. B. Walker, *Energy Environ. Sci.* **2016**, *9*, 1476.
[54] P. Calado, A. M. Telford, D. Bryant, X. Li, J. Nelson, B. C. O'Regan, P. R. F. Barnes, *Nat. Commun.* **2016**, *7*, 13831.
[55] M. H. Futscher, J. M. Lee, L. McGovern, L. A. Muscarella, T. Wang, M. I. Haider, A. Fakharuddin, L. Schmidt-Mende, B. Ehrler, *Mater. Horiz.* **2019**, *6*, 1497.
[56] N. Wu, D. Walter, A. Fell, Y. Wu, K. Weber, *J. Phys. Chem. C* **2020**, *124*, 219.
[57] D. W. deQuilettes, S. Koch, S. Burke, R. K. Paranji, A. J. Shropshire, M. E. Ziffer, D. S. Ginger, *ACS Energy Lett.* **2016**, *1*, 438.
[58] E. H. Jung, N. J. Jeon, E. Y. Park, C. S. Moon, T. J. Shin, T. Y. Yang, J. H. Noh, J. Seo, *Nature* **2019**, *567*, 511.
[59] Q. Jiang, Y. Zhao, X. Zhang, X. Yang, Y. Chen, Z. Chu, Q. Ye, X. Li, Z. Yin, J. You, *Nat. Photonics* **2019**, *13*, 460.
[60] W. S. Yang, B. Park, E. H. Jung, N. J. Jeon, Y. C. Kim, D. U. Lee, S. S. Shin, J. Seo, E. K. Kim, J. H. Noh, S. Il Seok, *Science* **2017**, *356*, 1376.
[61] M. Saliba, T. Matsui, K. Domanski, J.-Y. Seo, A. Ummadisingu, S. M. Zakeeruddin, J.-P. Correa-Baena, W. R. Tress, A. Abate, A. Hagfeldt, M. Grätzel, M. Gratzel, *Science* **2016**, *354*, 206.